Available online at www.sciencedirect.com
SCIENCE DIRECT®
Optics Communications 255 (2005) 286–296
OPTICS COMMUNICATIONS
www.elsevier.com/locate/optcom

Mutually delay-coupled semiconductor lasers: Mode bifurcation scenarios

H. Erzgräber [a,b,*], D. Lenstra [a,c], B. Krauskopf [b,a], E. Wille [d], M. Peil [d], I. Fischer [d], W. Elsäßer [d]

[a] *Afdeling Natuurkunde en Sterrenkunde, Vrije Universiteit Amsterdam, De Boelelaan 1081, 1081 HV Amsterdam, The Netherlands*
[b] *Department of Engineering Mathematics, Queen's Building, University of Bristol, Bristol BS8 1TR, UK*
[c] *Research Institute COBRA, Technical University Eindhoven, The Netherlands*
[d] *Institute of Applied Physics, Darmstadt University of Technology, Schloßgartenstraße 7, 64289 Darmstadt, Germany*

Received 3 February 2005; received in revised form 13 May 2005; accepted 3 June 2005

Abstract

We study the spectral and dynamical behavior of two identical, mutually delay-coupled semiconductor lasers. We concentrate on the short coupling-time regime where the number of basic states of the system, the compound laser modes (CLMs), is small so that their individual behavior can be studied both experimentally and theoretically. As such it constitutes a prototype example of delay-coupled laser systems, which play an important role, e.g., in telecommunication.

Specifically, for small spectral detuning we find several stable CLMs of the coupled system where both lasers lock onto a common frequency and emit continuous wave output. A bifurcation analysis of the CLMs in the full rate equation model with delay reveals the structure of stable and unstable CLMs. We find a characteristic bifurcation scenario as a function of the detuning and the coupling phase between the two lasers that explains experimentally observed multistabilities and mode jumps in the locking region.

PACS: 42.65.Sf; 05.45.Xt; 02.30.Ks; 42.55.Px

Keywords: Coupled semiconductor lasers; Delay-instabilities; Bifurcation analysis

1. Introduction

Systems of coupled semiconductor lasers (SLs) are receiving increasing interest, because of their practical importance, e.g., for achieving high out-

* Corresponding author.
E-mail address: h.erzgraber@few.vu.nl (H. Erzgräber).

0030-4018/$ - see front matter © 2005 Elsevier B.V. All rights reserved.
doi:10.1016/j.optcom.2005.06.016

put power or for on-chip integrated optical devices. Moreover, they are important examples of coupled oscillators in general. The spatial separation of the lasers always results in a time delay in the coupling due to finite signal propagation times. In many situations the time delay in the coupling has been neglected. However, for semiconductor lasers this is not always justified due to their large bandwidth and fast time scales of their dynamics. It is well known that delay effects can destabilize a system; see, e.g. [1]. In delay-coupled semiconductor lasers this may even result in chaotic dynamics as was shown in [2]. On the other hand, time delay in the coupling can also be used to stabilize a chaotic system [3]. This ambivalent character of delayed coupling makes this field attractive for fundamental investigations. Furthermore, delay-coupled SLs are promising candidates for different technological applications, such as secure chaos communication [4], ultra-fast optical clocks [5], and optical flip-flops [6].

The objective of our study is the generic case of two identical, mutually delay-coupled semiconductor lasers that receive each others light. Only the optical frequencies of the two lasers may differ, which leads to a detuning between the lasers. The delay τ in the coupling is then given by $\tau = L/c$, where L is the distance between the two lasers and c is the speed of light. We consider the case of the *short coupling time regime* as was introduced in [7] (for the case of a SL subject to conventional optical feedback). This means that the delay time τ is of the order of the period $T_{\mathrm{RO}} = \nu_{\mathrm{RO}}^{-1}$ of the characteristic relaxation oscillation – a periodic exchange between the number of photons and the number of electron–hole pairs (inversion).

Recently, a number of experimental and theoretical studies have been performed on this system. The dynamical behavior of delay-coupled SLs was found to be very different depending on the delay-time τ. Theoretical investigations for the limit of zero delay can be found in [8]. In [2] chaos synchronization in conjunction with symmetry breaking has been reported for long delay times. The dependence of the onset of chaos synchronization has been studied experimentally and numerically for different coupling strengths and injection currents in [9]. The limit of very large delay is the focus of theoretical studies in [10,11]. Numerical simulations are performed in [12] and an analytical formula is derived that predicts the oscillation frequency in the mode beating regime for short delays. Numerical investigations and an approximate thermodynamic potential can be found in [9,13]. For a short delay time of $\tau \approx \nu_{\mathrm{RO}}^{-1}$, regular dynamics, such as frequency locking with continuous wave emission and regular intensity oscillations, are dominant [14–16]. Depending on the detuning between the two lasers, a characteristic scenario has recently been demonstrated [16]. Increasing the detuning leads from optical frequency locking towards successive states of periodic intensity oscillations. A detailed bifurcation analysis in dependence on the detuning from the dynamical system can be found in [17]. The interesting question of the influence of the pump current, which effectively gives the transition from short to long coupling times, is discussed in [18].

In this paper, we report a detailed experimental study of the compound laser modes (CLMs) of two mutually delay-coupled SLs. We focus on the locking region in dependence of the detuning and the coupling phase between the lasers. Furthermore, we employ advanced methods from the bifurcation theory of delay differential equations (DDEs), in particular, numerical continuation of the CLMs with the package DDE-BIFTOOL [19]. The combination of experimental and theoretical techniques allows us to explain the observed dynamics, in particular, mode jumps and multistability leading to hysteresis loops. Hence, this paper proofs the existence of the CLMs experimentally as well as theoretically which lays the foundation for further studies of the dynamics of delay coupled SLs. Moreover, the good agreement between experiment and advanced bifurcation techniques shows the power of these techniques and opens the possibility to explain even complicated dynamics on a fundamental level. In turn this allows one to provide insight into the behavior of electro-optical systems. This is of importance because of the increasing interest in, e.g., multi-section laser devices.

More generally, our results contribute to the research on delay-coupled oscillators, which describe and explain widely differing phenomena, including chemical oscillations, biological clocks and

information processing in neural networks; see, for example [20–22] as entry points to the extensive literature on the subject. Phenomena that are attributed to time-delayed coupling include multistabilities, amplitude death and the onset of delay-induced instabilities [2,3,16,23].

The paper is organized as follows. In Section 2, we begin with a description of the system of coupled SLs and its experimental realization. Section 3 presents the experimental results, focusing on the influence of a detuning between the two SLs. Section 4 introduces the rate equation model of the system and the CLMs. Section 5 compares the bifurcation analysis with the experimental results. From this comparison we draw conclusions in Section 6, emphasizing the physical relevance of short-delay coupling induced locking-phenomena, and point to further work.

2. The system

We consider a system of two SLs that are mutually delay-coupled via the electromagnetic field. The two SLs are assumed to be identical, but they may have different solitary (i.e., in the absence of the other laser) optical frequencies leading to a spectral detuning between the two lasers.

In the experiment two SLs are placed in a face-to-face configuration as depicted in Fig. 1. We selected two 1540 nm single-mode distributed feedback (DFB) lasers. To achieve almost identical devices, both lasers where grown on the same wafer. The threshold currents are 9 mA. Both lasers have a linewidth enhancement factor α that has been determined to be about $\alpha = 2$, which is in the typical range for DFB laser used in telecommunication applications. The temperature of the lasers can be stabilized with an accuracy of better than 0.01 K. This allows for temperature induced frequency shifts with controllable steps smaller than 300 MHz. The lasers are pumped with two low-noise current sources.

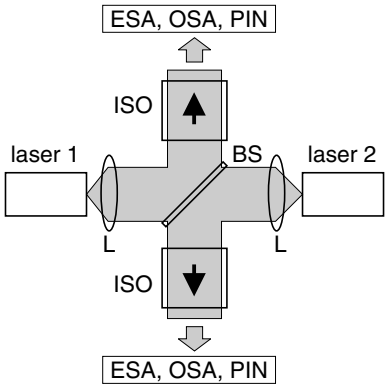

Fig. 1. Setup of the coupled laser system, including lenses L, beamsplitter BS, optical isolators ISO, electrical spectrum analyzer ESA, optical spectrum analyzers OSA, and pin-photodiodes PIN.

The beam of each laser is collimated by a lens (L), propagates along the coupling distance and is refocused into the active region of its opposing counterpart. A beamsplitter (BS) extracts 50% of the output power of each laser towards the measurement devices. The detection branches are separated from the SLs by two optical isolators (ISO) to suppress unwanted feedback. The optical spectra of the lasers are measured using two optical spectrum analyzers (OSA) with a relative resolution of better than 0.05 nm. To study the dynamical properties of the lasers the optical signal is converted into an electrical signal by a fast avalanche photodiode with a bandwidth of 12 GHz. The electrical signal is analyzed with an electrical spectrum analyzer (ESA). Additionally, the time-averaged output power of each laser is measured with two pin-photodiodes (PIN).

The optical pathlength between the lasers is $d = 51 \pm 1$ mm resulting in a delay of $\tau = 170 \pm 3$ ps. This delay corresponds to the round-trip frequency $f_{\text{ext}} = 2.9 \pm 0.1$ GHz. Although the scheme of the setup is conceptually simple, it is experimentally demanding: great care has been taken to achieve stable and well-defined coupling conditions. In particular, the short coupling distances force high demands on lateral, transverse, longitudinal and angular alignment. In a first step, the parallel alignment of the two lasers has been adjusted with the help of optical reflections. In a second step, the relative transverse and lateral positions of the lasers have been aligned by measuring the photocurrent that is induced in the respective other laser. Only if the dependence of the photocurrent is symmetric under variations

of the transverse and lateral position of each laser, it is assured that the light is coupled symmetrically into the active region of the lasers. Specially designed laser mounts have been used in order to achieve interferometric stability and full control over the coupling phase.

Special attention has been paid to determine the coupling strength and the possible influence of residual feedback that originates from reflections from the front facet of the other laser. By a consideration of the reflectivities, transmittivities and losses in the experimental setup, we have determined that approximately 5% of the output power of each laser is injected into the respective other laser. This was complemented and verified via measurements of the induced photocurrent. The residual feedback in our setup follows to be about two orders of magnitude smaller than the coupling. Nevertheless, one has to be aware that even very weak feedback of less than 0.1% can undamp relaxation oscillations in SLs [20]. Therefore, we measured the influences of the residual feedback in our coupling scheme by using one unpumped laser as a mirror. In the experiment we do not observe any dynamical behavior in the intensity spectra. The optical spectra exhibit unchanged lineshape when compared to single mode emission without residual feedback and we did not find side peaks due to relaxation oscillations. Thus, we conclude that in our experiment the residual feedback can be neglected.

To study how the behavior of the coupled laser system depends on a spectral detuning Δ we have chosen the following experimental procedure. The free-running optical frequency ν_1^0 of laser 1 is kept constant during the experiment, while the free-running optical frequency ν_2^0 of laser 2 is changed in small steps. This results in a variable spectral detuning $\Delta = \nu_2^0 - \nu_1^0$. Since we change Δ by detuning laser 2, this laser is called the *detuned laser*, while laser 1 is called the *unchanged laser*. The detuning Δ can be varied either by changing the temperature or the injection current of the detuned laser. Shifting the temperature yields a spectral detuning of approximately -12 GHz/K, while shifting the injection current yields a spectral detuning of approximately -1.1 GHz/mA. The exact dependence of the detuning on the injection current and the temperature is nonlinear; this nonlinear relationship was measured and used to determine the detuning. After each step of changing the detuning the optical spectra, the rf-spectra of the intensity dynamics, and the output intensity are recorded simultaneously. It is important that the coupling conditions remain constant within the measurement time. This is achieved by using laser mounts with thermal properties which allow a fast temperature stabilization and sufficient stability to accurately define the detuning conditions. We note that the presented results have been verified to be independent of the method of detuning, as well as to interchanging lasers 1 and 2.

3. Experimental results

In Fig. 2, we show the spectral shift of the detuned laser as white circles (○) and that of the unchanged laser as black circles (●). The detuning range was $-10 \leqslant \Delta \leqslant 10$ GHz, where the detuning has been achieved by varying the temperature of laser 2. To detect hysteresis effects, panel (a) is for increasing detuning and panel (b) for decreasing detuning as indicated with arrows. We define increasing detuning as the positive detuning direction and decreasing detuning as the negative detuning direction.

The spectral shift is defined as the difference $\eta_{1,2} = \nu_{1,2} - \nu_{\text{stat}}^0$ between the optical frequency $\nu_{1,2}$ of the respective laser in the coupled system and the free-running frequency ν_{stat}^0 of the unchanged laser. The lasers were pumped at 6.5 times their threshold; for this pump current their relaxation oscillation frequency has been extrapolated to be about 15 GHz.

In Fig. 2 one can distinguish two different regimes. For a detuning near $\Delta = 0$ both lasers are locked to the same optical frequency, i.e., $\eta = \eta_1 = \eta_2$. In this locking region we do not measure any intensity dynamics in the rf-spectra and the lasers emit on a single optical mode. Small deviations between the measured spectral positions of both lasers in Fig. 2 are due to the limited resolutions of the OSAs. Outside this locking region both lasers emit with different frequencies, i.e., $\eta_1 \neq \eta_2$. This region is indicated by a grey background.

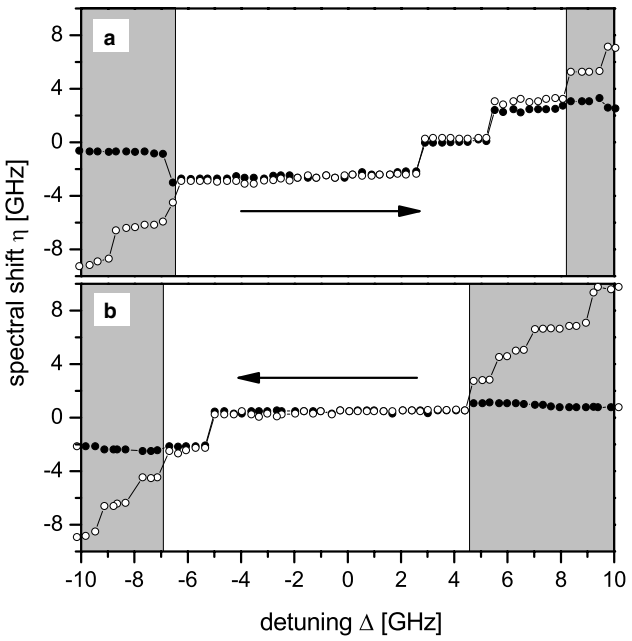

Fig. 2. Spectral shift η of both lasers for positive (a) and negative (b) detuning direction. White circles (○) indicate the detuned laser and black circles (●) the unchanged laser. A grey background indicates regions with oscillating intensity dynamics outside the locking region.

Here the intensity of both lasers oscillates with a frequency equal to their spectral separation $|\eta_2 - \eta_1|$. A detailed discussion of the oscillatory behavior outside the locking region can be found in [16]. Here, we focus on the locking region. For the positive detuning direction, shown in Fig. 2(a), the locking region ranges from $\Delta = -6.4$ GHz to $\Delta = 8.2$ GHz. Inside the locking region we observe three steps of constant frequency situated at about $\eta = -2.5$ GHz, $\eta = 0.1$ GHz and $\eta = 2.5$ GHz, while the steps cover a detuning range of 9.1, 2.7 and 2.8 GHz, respectively. When increasing Δ, the width of the first step of the locking region is more than three times larger than that of the other two steps. For decreasing detuning, shown in Fig. 2(b), the locking region is shifted towards lower values of the detuning within $-6.9 \leqslant \Delta \leqslant 4.6$ GHz. Here, the locking region consists of two steps. The first is situated at about $\eta = 0.4$ GHz and the second at $\eta = -2.1$ GHz. Again, the first step covers a detuning range of 9.8 GHz and is much larger than the second step that covers 1.7 GHz. Comparing Figs. 2(a) and (b) one can see that, within the experimental accuracy, the small step for the negative detuning direction has the same spectral position η as the large step for the positive detuning direction. In fact, both overlap around $\Delta = -6$ GHz. The same holds around $\Delta = 4$ GHz.

We conclude from these experimental results that the three steps within the locking region correspond to three stable modes of the delay-coupled laser system. Therefore, we denote these modes as *compound laser modes* (CLMs). As is evidenced in Fig. 2, the CLMs exhibit multistabilities. First, two of the CLMs overlap over a detuning range of about 8 GHz which results in the observed hysteresis of the two large steps. Second, at the border of the locking region the CLMs overlap with oscillating states of the coupled laser system. This results in the discrepancies of the observed locking boundaries depending on the detuning direction. The frequency separation between the CLMs of 2.4 and 2.5 GHz, respectively, is related to the round trip frequency $f_{\text{ext}} = 2.9$ GHz of the system. However, there are two physical reasons for the deviation of the CLM separation from f_{ext}. First, the mode separation of two delay-coupled laser

resonators has been shown to be smaller than its round trip frequency [24] which is mainly due to coupling losses. Second, mutual frequency pulling between the two lasers influences the mode separation of the coupled system. This effect is similar to the well-known frequency pulling for SLs with external optical injection [25]. For a full description of the structure of the CLMs, the nonlinearities of the SLs need to be included in the model. This is the topic of Section 4.

We now take a more detailed look at the individual CLMs. Fig. 3(a) depicts the spectral shift of the lasers inside the locking region for the negative detuning direction. For simplicity, only the spectral shift of the unchanged laser is shown as both lasers are frequency locked. The dashed line indicates the free running frequency of the detuned laser. In Fig. 3 the detuning was achieved by increasing the pump current of the detuned laser between 36 and 47 mA, where $\Delta = 0$ corresponds to 40 mA. The unchanged laser was pumped at 40 mA. Fig. 3(b) depicts the output power of the unchanged and the detuned lasers. For comparison, the output power of the uncoupled detuned laser is indicated by the continuous line.

The output power of the unchanged laser remains almost constant on each CLM. When the coupled SLs jump towards a CLM at a lower optical frequency the power of the unchanged laser decreases by about 20% at each mode jump. The power of the detuned laser does not remain constant on one CLM but increases in the negative detuning direction. This increase is not due to the increasing injection current alone: the slope of the power is significantly steeper for the detuned laser as compared to solitary operation. In fact, the output power of both lasers depends on the difference between the frequency of the coupled laser system $\nu = \nu_1 = \nu_2$ and the frequency of the respective solitary laser $\nu^0_{1,2}$. With increasing difference $\nu - \nu^0_{1,2}$, the power of the respective laser increases. If $\nu - \nu^0_{1,2}$ changes into the negative direction, the power of the respective laser decreases. A change of $\nu - \nu^0_{1,2}$ originates from two

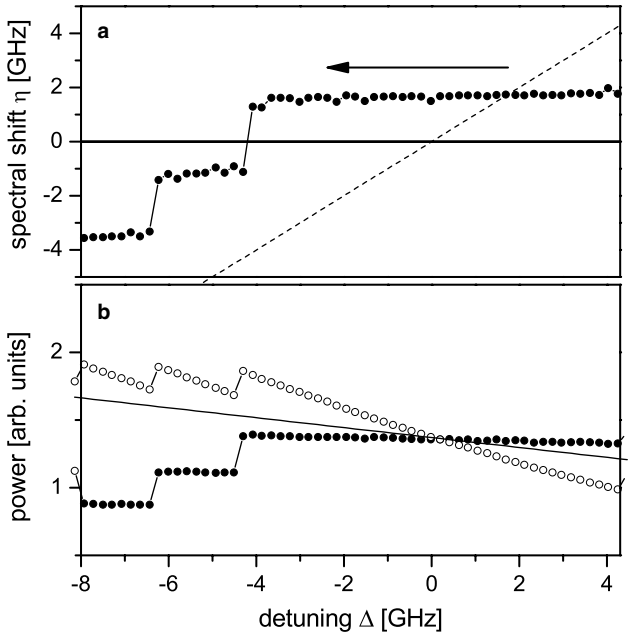

Fig. 3. Spectral shift η of the unchanged laser (a) and measured output power (b) of both lasers in the locking regime; white circles (○) are for the detuned laser and black circles (●) for the unchanged laser. The detuning was achieved by changes in the pump current of laser 2; in (a) the free-running frequency shift of the detuned laser is indicated with a dashed line, and in (b) the continuous line indicates the output power of the uncoupled detuned laser.

distinct mechanisms: in the case of the unchanged laser, only mode jumps result in changes of ν. For the detuned laser, in addition to mode jumps, a change of $\nu - \nu_{1,2}^0$ occurs also due to the variation of ν_2 (i.e., the detuning). Therefore, in the latter case the steps of the output power exhibit an underlying slope. Corresponding mode jumps (in different positions due to the hysteresis) are found for the other detuning direction.

4. Rate equation model

We model the coupled laser system with rate equations for the normalized complex slowly varying envelope of the optical fields $E_{1,2}$ and the normalized inversions $N_{1,2}$. As for the Lang–Kobayashi rate equations for a laser with conventional optical feedback [26], the main modeling assumption is that the feedback rate is small enough so that multiple roundtrips can be neglected. See [27] for a detailed derivation of these equations, which can be written in dimensionless form as

$$\frac{dE_1}{dt} = (1 + i\alpha)N_1E_1 + \kappa e^{-i\Omega_1\tau_n}E_2(t - \tau_n), \tag{1}$$

$$\frac{dE_2}{dt} = (1 + i\alpha)N_2E_2 + \kappa e^{-i\Omega_1\tau_n}E_1(t - \tau_n) + i\delta E_2, \tag{2}$$

$$T\frac{dN_1}{dt} = P - N_1 - (1 + 2N_1)|E_1|^2, \tag{3}$$

$$T\frac{dN_2}{dt} = P - N_2 - (1 + 2N_2)|E_2|^2. \tag{4}$$

Eqs. (1)–(4) are written in the reference frame of the unchanged laser, i.e., laser 1. Thus the optical fields of the lasers are represented by $E_i(t)e^{i\Omega_1 t}$, where Ω_1 is the optical angular frequency of laser 1 operated solitary at threshold. The time t is measured in units of the photon lifetime. Apart from the difference in their solitary optical frequencies, the two lasers are considered to be identical.

The mutual coupling is given by the second term of Eqs. (1) and (2). It contains the coupling strength κ, the delay time τ_n and the coupling phase $C_p = \Omega_1\tau_n$. The detuning between the two lasers is taken into account by the last term of (2) where $\delta = (\Omega_2 - \Omega_1)$, and Ω_2 is the optical angular frequency of the second laser operated solitary at threshold. It is an important observation that the coupling phase C_p depends very sensitively on τ_n and Ω_1: tiny changes of τ_n and Ω_1 lead to substantial changes of C_p. Therefore, it makes sense to consider C_p as an independent parameter. This is helpful in the mathematical analysis and in good agreement with the experiment. Note that C_p is the analogue of the feedback phase in the Lang–Kobayashi equations for a laser with conventional optical feedback, which is also often considered to be an independent parameter for the same reasons; see, e.g. [28,29].

The remaining parameters are the linewidth enhancement factor α, the coupling strength κ, the normalized carrier lifetime T and the pump parameter P. We consider here the values $\tau_n = 25.49$, $\alpha = 2.0$, $\kappa = 0.047$, $T = 150.0$, and $P = 13.17$, which were derived from the physical values in Table 1.

As in the case of the Lang–Kobayashi equations [26], the basic solution of (1)–(4) are continuous wave solutions which we call CLMs. They can be written in the following form:

$$E_1(t) = R_1^s e^{i\omega^s t}, \quad E_2(t) = R_2^s e^{i\omega^s t + i\sigma},$$
$$N_1(t) = N_1^s, \quad N_2(t) = N_2^s, \tag{5}$$

where R_i^s, N_i^s, ω^s, and σ are time independent and real valued. Furthermore, the R_i^s are taken to be positive. The lasers must have the same frequency ω^s but there may be some time-independent phase shift σ between them. Furthermore, the lasers may have different steady state amplitudes R_i^s and different steady state inversions N_i^s. Physically, a CLM corresponds to a frequency locked state where the two lasers have constant output power; compare Section 3. It is important to note that

Table 1
Laser parameters and their values

Laser parameter	Value
α-parameter	2.0
Photon decay rate	150 ns^{-1}
Electron decay rate	1 ns^{-1}
Differential gain	790 s^{-1}
Coupling rate	7 ns^{-1}
Coupling time	0.17 ns
Pump current	6 × threshold
Carrier density at threshold	10^{18}

CLMs are periodic orbits in phase space. However, they are special in that the periodicity is due to the S^1-symmetry of the system (1)–(4) of rotation of both E_1 and E_2 (over any angle). As a consequence, R_i^s and N_i^s are constant; see [17] for details. (Mathematically, a CLM is a group orbit of the S^1-symmetry.) In particular, in a rotating frame with frequency ω^s, a CLM is a single point. The situation is conceptually the same as that for the Lang–Kobayashi equations of a laser with conventional optical feedback, where the external cavity modes are periodic orbits due to S^1-symmetry [29,30].

The main difficulty for any analysis is that Eqs. (1)–(4) are a system of delay differential equations (DDEs). Consequently, their phase space is the space of continuous functions over the delay interval $[-\tau_n, 0]$; see [31,32]. This reflects the fact that one needs as initial condition not only the present time point but also the entire history of length τ_n – in the case of Eqs. (1)–(4) the values of E_1, E_2, N_1 and N_2 over $[-\tau_n, 0]$.

We use the approach of considering individual CLMs as starting data for the numerical continuation of CLMs with the package DDE-BIFTOOL [19]. This software allows one to find and follow (or continue) branches of equilibria and periodic solutions. Stability information is computed along such branches so that basic bifurcations can be detected. We mention here briefly that DDE-BIFTOOL requires solutions to be isolated. Therefore, to compute branches of CLMs one must fix the phase of the CLM under consideration. Effectively one picks one CLM in the group orbit of the S^1-symmetry. This is done here as in [33,34], where further details can be found.

Bifurcation analysis of delay equations with numerical continuation is a very powerful tool [35]. In terms of the system at hand, it can be used to give a detailed description of the bifurcation structure of the CLMs in terms of the mutual effect of detuning and feedback phase. This structure is organized by the case of zero detuning, which features the additional phase-space symmetry of exchanging the two lasers. When the pump current is sufficiently far above threshold (as is also the case in this paper) there is a typical scenario; see [17]. Note that the influence of the pump current on the CLM structure is discussed in detail in [18].

5. Dependence of CLMs on the detuning

In this paper, we present a bifurcation study that is limited to the direct vicinity of the locking region of the system, in analogy to the shown experiments. Specifically, we study how the structure of the CLMs of Eqs. (1)–(4) changes when the detuning δ is allowed to vary freely in the positive or negative direction. As it was done in the experiments described in Section 2, we keep the frequency Ω_1 of laser 1 fixed and change the frequency Ω_2 of laser 2. Of particular interest is how stable regions change with the feedback phase C_p.

Fig. 4 shows the CLMs in the (Ω_2, ω^s)-plane for six different values of C_p; from panels (a) to (f) the coupling phase C_p decreases from 0 to $-\frac{5}{6}\pi$. Each panel shows a closed self-intersecting curve. The exact shape depends on the value of C_p, and the sequence repeats after C_p has been changed by π. CLMs are born and lost in saddle-node bifurcations as Ω_2 is increased or decreased. For each value of C_p there are multiple stable regions, which may overlap. The boundaries of a stable region

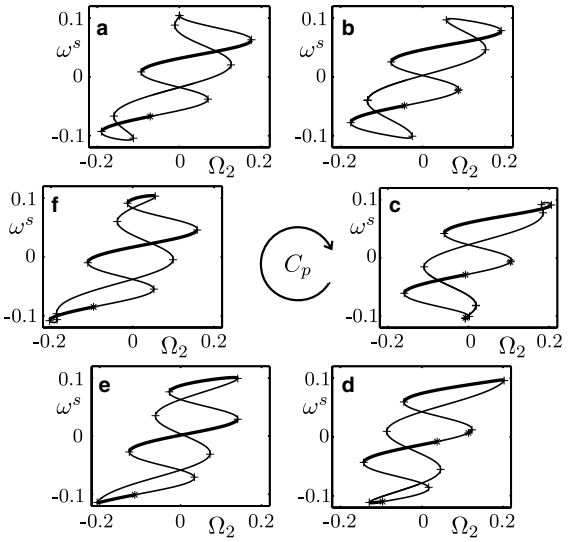

Fig. 4. CLMs in the (Ω_2, ω^s)-plane and their dependence on the feedback phase C_p. From (a) to (f) C_p takes values from 0 to $-\frac{5}{6}\pi$. Saddle-node bifurcations are marked by pluses (+) and Hopf bifurcations by stars (∗); stable regions are plotted as thick curves.

are typically formed by a saddle-node bifurcation on one side and a saddle-node or Hopf bifurcation on the other side. The intensities $I^s_{1,2} = (R^s_{1,2})^2$ of the CLMs depend on the detuning in a similar way. Indeed, a plot of the intensities of the lasers corresponds to a different projection of the curves of CLMs shown in Fig. 4. In particular, the stability regions agree.

In Figs. 5(a) and (b1)/(b2), we show the CLMs in projection onto the (Ω_2, ω^s)-plane and the (Ω_2, I^s_1)- and (Ω_2, I^s_2)-planes, respectively, for the value of $C_p = 0.63\pi$. Note that it is not possible to determine the absolute value of C_p in the experiment. The value of $C_p = 0.63\pi$ was chosen because it represents the best agreement with the experimental measurements shown in Figs. 2 and 3(b). We remark that we performed more measurements than shown, which verify the dependence on the coupling phase C_p as illustrated in Fig. 4.

To interpret the theoretical Figs. 5(a) and (b1)/(b2) in terms of the experimental measurements shown in Fig. 3 one needs to consider only the stable (bold) branches. The mode jumps observed in the experiment, when Ω_2 is decreased, correspond to the left endpoints of stable branches. This is illustrated in Figs. 5(c) and (d), which show what is observed in terms of the frequency ω and the intensities $I_{1,2}$ when the rightmost stable CLM is followed for decreasing Ω_2. Specifically, the rightmost stable CLMs is born in a saddle-node bifurcation at $\Omega_2 \approx 0.16$, and it corresponds to stable locking where both lasers exhibit stable emission with the common frequency ω^s. This frequency changes slightly as Ω_2 decreases (Figs. 5(a) and

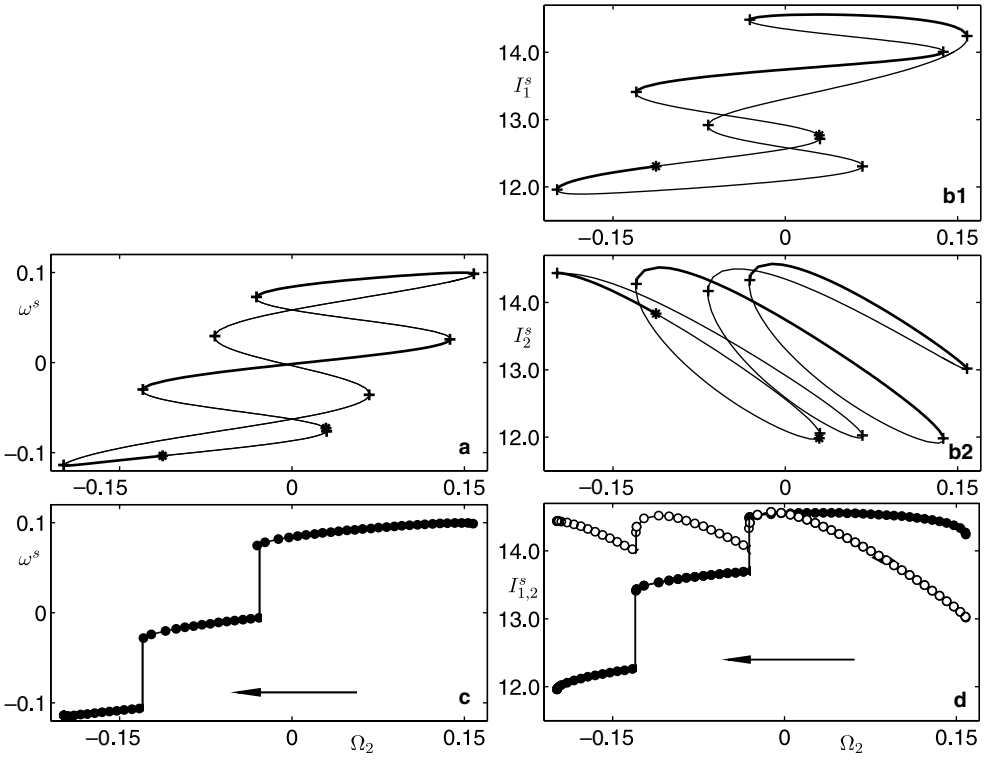

Fig. 5. Full branches of CLMs for C_p=0.63π in the (Ω_2, ω^s)-plane (a), the (Ω_2, I^s_1)-plane (b1) and the (Ω_2, I^s_1)-plane (b2). Saddle-node bifurcations are marked by pluses (+) and Hopf bifurcations by stars (*); stable regions are plotted as thick curves. Panels (c) and (d) show the parts of the branches that are followed for decreasing detuning. In (d) black circles (•) are for laser 1 and white circles (○) for laser 2.

(c)). Notice that the intensity of the unchanged laser remains almost constant (Figs. 5(b1) and (d)), while that of the detuned laser increases with decreasing Ω_2 (Figs. 5(b2) and (d)). This stable CLM disappears in a saddle-node bifurcation at $\Omega_2 \approx -0.03$ and the system 'drops down' onto the middle stable branch of stable CLMs (Figs. 5(c) and (d)). The lasers' frequency ω^s and the intensities I_1^s of the unchanged and I_2^s of the detuned laser are now lower. When Ω_2 is decreased further, ω^s and I_1^s remain almost constant, while I_2^s increases. In the saddle-node bifurcation at $\Omega_2 \approx -0.13$ also this CLM disappears and the system drops to the lower stable branch of CLMs. The frequency ω^s of the coupled laser system is now at an even lower frequency, again almost constant. Also the intensities I_1^s and I_2^s drop in value. Finally, this CLM disappears in the saddle-node bifurcation at $\Omega_2 \approx -0.2$ and the system leaves the locking region. The steps and the jumps in the measured frequency and intensities in Fig. 3 are well explained by this scenario.

As it is clear from Figs. 5(a) and (b1)/(b2), owing to hysteresis loops the jumps between CLMs will take place at different values when Ω_2 is increased. This explains the jumps in the intensity at different values of Ω_2 depending on the direction of scanning in the experimental measurements in Fig. 2. Note that multistability and hysteresis loops occur irrespective of the value of C_p, as can be seen from the panels of Fig. 4.

Finally, we would like to point out already two other sources of multistability and possible hysteresis loops, which are both beyond the scope of this paper. First, there may be multistability between CLMs and periodic solutions that can emerge from Hopf bifurcations *within the locking region* (when they are supercritical). Depending on the value of C_p there may be small regions of (small amplitude) oscillations inside the locking region. Second, there is multistability between stable locking and the dynamics *outside the locking region*. This has also been observed in experiments, and it is responsible for the different size of the region of measured stable locked dynamics in Figs. 2(a) and (b). These two effects may, in fact, be in competition. For example, we found that the Hopf bifurcation bounding the lowest step to the right in Figs. 5(a) and (b1)/(b2) is supercritical. However, the locking region is entered even later for increasing Ω_2 because the system is still in another dynamical state that loses its stability for even larger Ω_2. This hints at an interesting interplay of other stable dynamics with the underlying CLM structure as discussed here. The exact nature of this interplay is a topic of ongoing research.

6. Conclusions

We have provided a detailed characterization of a system of two SLs that are mutually coupled via the electromagnetic field. The delay time in the coupling due to the spatial distance between the lasers gives rise to a characteristic structure of compound laser modes (CLM). For small detuning we found multistabilities between different modes where both lasers lock to a common optical frequency and exhibit stable emission. When changing the detuning between the lasers we observed that the coupled laser system undergoes mode jumps to other stable CLMs within the locking region. The multistability of the CLMs has been experimentally evidenced by the observation of hysteresis for positive and negative detuning directions. A second kind of multistability between the locking region and the regime with oscillating intensity dynamics outside the locking was found in the experiment. Additionally, we showed how the output intensity of each laser on an individual mode depends on the detuning.

For a deeper understanding, we used a rate equation model to study the underlying structure of the CLMs using numerical continuation of the full DDE system. Focusing on the locking region around zero detuning, multiple stable CLMs are found. They typically destabilize via a saddle node bifurcation that give rise to the observed hysteresis loops. However, destabilization is also possible in Hopf bifurcations, some of which may give rise to amplitude oscillations. How this dynamics interacts with the stable CLMs is ongoing research.

Our analysis focused on the locking region around zero detuning and the local bifurcations found there. We find good qualitative agreement

between experiment and theory. In particular, our results show the importance of the coupling phase C_p. The next step is to understand the dynamics outside the locking region and different scenarios on the route to locking. Preliminary investigations suggest that this requires the study of global structures in phase space, which is an interesting topic in its own right. At the same time, it will bring to light dynamical effects that are crucial for understanding the performance of coupled laser systems.

Acknowledgment

The authors thank Nortel Networks for providing the excellent DFB lasers.

References

[1] G. Stépán, Retarded Dynamical Systems: Stability and Characteristic Functions, Longman Scientific and Technical, London, UK, 1989.
[2] T. Heil, I. Fischer, W. Elsäßer, J. Mulet, C.R. Mirasso, Phys. Rev. Lett. 86 (2001) 795.
[3] D.V. Ramana Reddy, A. Sen, G.L. Johnston, Phys. Rev. Lett. 80 (1998) 5109.
[4] I. Fischer, Y. Liu, P. Davis, Phys. Rev. A 62 (2000) 011801.
[5] M. Möhrle, B. Sartorius, C. Bornholdt, S. Bauer, O. Brox, A. Sigmund, R. Steingrüber, M. Radziunas, H.-J. Wünsche, IEEE J. Sel. Top. Quantum Electron. 7 (2001) 217.
[6] M.T. Hill, H. de Waardt, H.J.S. Dorren, IEEE J. Quantum Electron. QE-37 (2001) 405.
[7] T. Heil, I. Fischer, W. Elsäßer, A. Gavrielides, Phys. Rev. Lett. 87 (2001) 243901.
[8] S. Yanchuk, K. Schneider, L. Recke, Phys. Rev. E 69 (2004) 056221.
[9] J. Mulet, C. Mirasso, T. Heil, I. Fischer, J. Opt. B 6 (2004) 97.
[10] J. Javaloyes, P. Mandel, D. Pieroux, Phys. Rev. E 67 (2003) 036201.
[11] E.A. Viktorov, A.M. Yacomotti, P. Mandel, J. Opt. B 6 (2004) L9.
[12] F. Rogister, J. García-Ojalvo, Opt. Lett. 28 (2003) 1176.
[13] R. Vicente, J. Mulet, M. Sciamanna, C. Mirasso, Proc. SPIE 5349 (2004) 307.
[14] A. Hohl, A. Gavrielides, T. Erneux, V. Kovanis, Phys. Rev. Lett. 78 (1997) 4745.
[15] A. Hohl, A. Gavrielides, T. Erneux, V. Kovanis, Phys. Rev. A 59 (1999) 3941.
[16] H.-J. Wünsche, S. Bauer, J. Kreissl, O. Ushakov, N. Korneyev, F. Henneberger, E. Wille, H. Erzgräber, M. Peil, W. Elsäßer, I. Fischer, Phys. Rev. Lett. 94 (2005) 163901.
[17] H. Erzgräber, B. Krauskopf, D. Lenstra, Applied Nonlinear Mathematics Research Report 2004.28. Available from: <http://www.enm.bris.ac.uk/anm/preprints/2004r28.html> (submitted).
[18] H. Erzgräber, B. Krauskopf, D. Lenstra, Applied Nonlinear Mathematics Research Report 2005.9. Available from: <http://www.enm.bris.ac.uk/anm/preprints/2005r09.html> (submitted).
[19] K. Engelborghs, T. Luzyanina, G. Samaey, Technical Report TW-330, Department of Computer Science, K.U. Leuven, Leuven, Belgium, 2001.
[20] S.H. Strogatz, I. Stewart, Sci. Am. 269 (12) (1993) 68.
[21] S.H. Strogatz, Nonlinear Dynamics and Chaos, Perseus Books, Reading, Massachusetts, 1994.
[22] A. Pikovsky, M. Rosenblum, J. Kurths, Synchronization: A Universal Concept in Nonlinear Sciences, Cambridge University Press, Cambridge, 2001.
[23] H. Schuster, P. Wagner, Progr. Theor. Phys. 81 (1989) 939.
[24] G.C. Dente, C.E. Moeller, P.S. Durkin, IEEE J. Quantum Electron. 26 (1990) 1014.
[25] G.H.M. van Tartwijk, A.M. Levine, D. Lenstra, IEEE J. Sel. Top. Quantum Electron. 1 (1995) 466.
[26] R. Lang, K. Kobayashi, IEEE J. Quantum Electron. QE-16 (1980) 347.
[27] J. Mulet, C. Masoller, C.R. Mirasso, Phys. Rev. A 65 (2002) 063815.
[28] T. Heil, I. Fischer, W. Elsäßer, B. Krauskopf, K. Green, A. Gavrielides, Phys. Rev. E 67 (2003) 066214.
[29] V. Rottschäfer, B. Krauskopf, in: 5th IFAC Workshop on Time-Delay Systems, 2004.
[30] B. Krauskopf, G.H.M. van Tartwijk, G.R. Gray, Opt. Commun. 177 (2000) 347.
[31] J.K. Hale, S.M.V. Lunel, Introduction to Functional Differential Equations, Springer, New York, 1993.
[32] O. Diekmann, S.A.V. Gils, S.M.V. Lunel, Delay Equations: Functional-, Complex-, and Nonlinear Analysis, Springer, New York, 1995.
[33] B. Haegeman, K. Engelborghs, D. Rose, D. Pieroux, T. Erneux, Phys. Rev. E 66 (2002) 046216.
[34] B. Krauskopf, H. Erzgräber, D. Lenstra, in: 5th IFAC Workshop on Time-Delay Systems, 2004.
[35] B. Krauskopf, Bifurcation analysis of lasers with delay, in: D.M. Kane, K.A. Shore (Eds.), Unlocking Dynamical Diversity: Optical Feedback Effects on Semiconductor Lasers, Wiley, New York, 2005, pp. 147–183.